Quaternary Geochronology 12 (2012) 87–97

Contents lists available at SciVerse ScienceDirect

Quaternary Geochronology

journal homepage: www.elsevier.com/locate/quageo

Research paper

Evaluating a SAR TT-OSL protocol for dating fine-grained quartz within Late Pleistocene loess deposits in the Missouri and Mississippi river valleys, United States

Nathan D. Brown*, Steven L. Forman

University of Illinois at Chicago, Earth and Environmental Sciences, 845 W. Taylor St., Chicago, IL 60607-7059, USA

ARTICLE INFO

Article history:
Received 18 April 2012
Received in revised form
25 June 2012
Accepted 29 June 2012
Available online 20 July 2012

Keywords:
TT-OSL
OSL
Luminescence
Loess
Marine oxygen-isotope stage
Mississippi river

ABSTRACT

The Mississippi and Missouri river valleys in the midcontinental United States contain extensive loess-paleosol sequences that are used to constrain the timing of expansion and retreat of the Laurentide Ice Sheet. Previous studies have been unsuccessful in producing finite ages for sediments older than ~150 ka due to saturation of luminescence emissions. The thermally transferred optically stimulated luminescence (TT-OSL) dating technique is tested on the fine-grained (4–11 μm) quartz fraction of these loess deposits because the TT-OSL signal has been shown to grow with high (kGy) radiation doses. The TT-OSL signal continued to increase with radiation dose above 900 Gy. The optical and thermal stabilities of this TT-OSL signal are evaluated. Equivalent dose values are highly sensitive to preheat temperatures. Recycling ratios, zero-dose response values, and dose recovery tests all yield acceptable values for samples with burial doses >~200 Gy. The apparent TT-OSL ages for the Roxana Silt (~52–63 ka), Teneriffe Silt (~66 ka), and Loveland Silt (~133–192 ka) agree at 1σ level with previously published TL and IRSL ages derived from the same samples. For the oldest unit, the Crowley's Ridge Silt, TT-OSL ages (~167–200 ka) are younger than IRSL or TL ages by ~20%. This is interpreted as underestimation related to TT-OSL signal contamination, which can be avoided by isolating the fast component of the TT-OSL. Preliminary fast component TT-OSL ages for the Crowley's Ridge Silt (~197–241 ka) favor deposition during marine oxygen-isotope stage (MIS) 7 or 8, contrary to a previous inference of a MIS 12 deposition.

1. Introduction

In mid- to high- latitude regions, an important palaeoclimate record is wind-blown dust (loess) modified by pedogenic processes (Catt, 1991; Begét, 2001). The more complete glacigenic loess-palaeosol sequences reflect a changing balance between pedogenesis and loess accumulation which, in turn, reflects variable moisture conditions and sediment supply often within a glaciofluvial environment (Kemp, 2001). Chronologic control of these sequences provides insights on the timing of past glaciations, associated semi-arid conditions (e.g., Bettis et al., 2003; Wang et al., 2009) and can also test hypotheses on lead or lag times between aeolian deposition and larger climatic controls, such as insolation or oceanic cooling (e.g., Muhs et al., 2008).

The Missouri, Mississippi, Wabash and Ohio river valleys in the central USA contain at least four (Blum et al., 2000) and possibly up to seven (Follmer, 1983, 1996) major loess deposits. These aeolian deposits are probably sourced from proglacial fluvial and lacustrine surfaces associated with the expansion and retreat of the Laurentide Ice Sheet into midcontinental North American (cf. Markewich et al., 1998; Forman and Pierson, 2002; Bettis et al., 2003). Aeolian deposition during the last glaciation in North America spanned most of the glacial-to-deglacial cycle (e.g., Forman and Pierson, 2002; Bettis et al., 2003; Mason et al., 2011). The chronology of loess deposition and inferred timing of subsequent soil formation in the midcontinental USA have been evaluated by radiocarbon (Snowden and Priddy, 1968; McKay, 1979; Follmer, 1983; Forman et al., 1992; Wang et al., 2009), thermoluminescence (TL) (Forman et al., 1992; Rodbell et al., 1997; Markewich et al., 1998), infrared stimulated luminescence (IRSL) (Forman and Pierson, 2002), blue-light optically stimulated luminescence (OSL) (Forman and Pierson, 2002) and uranium-series isochron (Wang et al., 2009) dating methods. The youngest loess deposit is the Peoria Loess with a calendar-corrected radiocarbon age of ~12–25 ka (Snowden and Priddy, 1968; McKay, 1979; Follmer, 1983; Leigh and Knox, 1992; Forman and Pierson, 2002). The next

* Corresponding author. Tel.: +1 312 869 0435; fax: +1 312 413 2279.
E-mail address: nathan.david.brown@ucla.edu (N.D. Brown).

1871-1014/$ – see front matter © 2012 Elsevier B.V. All rights reserved.
http://dx.doi.org/10.1016/j.quageo.2012.06.008

oldest loess, separated from the Peoria Loess by the Farmdale Geolsol, is the Roxana Silt deposited ~30–55 ka (McKay, 1979; Follmer, 1983; Leigh and Knox, 1992; Forman et al., 1992; Rodbell et al., 1997; Markewich et al., 1998; Wang et al., 2009). The Loveland Loess, often associated with the Illinoian Glaciation and stratigraphically separated from the Roxana Silt by the Sangamon Geosol yielded a range of luminescence ages on polymineral and quartz extracts of ~110–180 ka (Maat and Johnson, 1996; Rodbell et al., 1997; Markewich et al., 1998; Forman and Pierson, 2002). The polymineral fraction from the Teneriffe Silt, a supposed correlative deposit to the Loveland Loess, yielded younger TL and IRSL ages of ~70–100 ka (Forman and Pierson, 2002). One of the oldest suspected pre-Illinoian loess in the middle Mississippi Valley is the Crowley's Ridge Silt, which lies below the Loveland Loess and the prominent Yarmouth Paleosol and yielded minimum-limiting IRSL and TL ages from the fine-grained (4–11 μm) polymineral extract of >~159–274 ka, probably reflecting saturation of the additive dose response (Forman and Pierson, 2002). The previous luminescence ages on the Loveland Loess and Crowley's Ridge Silt may be unreliable because of the use of low temperature (125 °C) infrared emissions from the polymineral fraction which may fade, even with rigorous preheat treatments and storage prior to analysis (e.g., Lamothe et al., 2003; Buylaert et al., 2007; Murray et al., 2009), in addition to inaccuracies associated with extrapolation of equivalent dose (and thus age) by additive dose methods, particularly near the saturation dose.

Fortunately, recent studies have used the thermally-transferred charge within quartz to date sediments as old as ~1 Ma (Wang et al., 2007; Tsukamoto et al., 2008; Porat et al., 2009; Stevens et al., 2009). The relevant portion (recuperated signal, or ReOSL) of the thermally transferred optically stimulated luminescence (TT-OSL) signal grows with high (~3.78 kGy) radiation doses (Wang et al., 2006), and resets with prolonged (hours to days) sunlight exposure (Pagonis et al., 2008), both necessary conditions for dating loess deposits. Moreover, recent advances to the TT-OSL method, including the development of single aliquot regenerative (SAR) protocols (Wang et al., 2007; Tsukamoto et al., 2008; Porat et al., 2009; Stevens et al., 2009; Adamiec et al., 2010), indicate that this technique may be suitable for dating a variety of aeolian depositional settings for most of the Quaternary (Kim et al., 2009; Rosenberg et al., 2011; Jacobs et al., 2011). Therefore, in this study we test the accuracy and precision of modified SAR TT-OSL protocols to date the fine-grained (4–11 μm) quartz fraction of common loess deposits in midcontinental North America spanning the past ~500 ka.

2. Sample context and measurements

Common loess deposits within the Mississippi and Missouri river basins are well-expressed at the Bonfils Quarry section, the Loveland Loess type locality and the Pleasant Grove School section (Fig. 1). From these sites, five representative loess units were studied: the Peoria Loess, the Roxana Silt, the Loveland Silt, the Teneriffe Silt, and the Crowley's Ridge Silt (Forman and Pierson, 2002). Quartz grains from twelve previously collected loess samples (Forman et al., 1992; Forman and Pierson, 2002) were prepared for analysis.

The fine-grained (4–11 μm) quartz was extracted from all samples under subdued yellow light (Na-vapor bulb) conditions. Samples were pretreated for 24 h with 11.1% HCl and 30% H_2O_2 to remove carbonates and organic material, respectively. The fine silt fraction (4–11 μm) was isolated using physical separation methods based on Stokes' Law. Finally, the polymineral sediment was immersed in silicon-saturated hexafluorosilicic acid (H_2SiF_6) for six days to isolate the quartz component (Berger et al., 1980; Roberts, 2007). To ensure the purity of the quartz separate, the ratio of IR luminescence-to-blue-light luminescence was examined after the H_2SiF_6 treatment: if the ratio was >0.1, samples underwent a second H_2SiF_6 treatment to render a pure quartz separate.

Dose-rate calculations were based on U, Th, and K concentrations and the conversion factors of Adamiec and Aitken (1998). U and Th contents were determined using thick-source alpha counting, assuming secular equilibrium based on comparisons between unsealed and sealed bulk alpha count rates (Sjostrand and Prescott, 2002). The K_2O concentrations were measured by Activation Laboratories LTD, Ontario, Canada using inductively-coupled plasma mass spectrometry. An a-value of 0.06 ± 0.02 was used for all samples, similar to IRSL values (Forman and Pierson, 2002). Also included in the dose-rate calculation was a small (0.12 ± 0.02 Gy/ka) cosmic ray component (Prescott and Hutton, 1994), and a moisture content of 15 ± 5% (by weight) based upon in situ measurements of water content (Forman and Pierson, 2002).

All luminescence measurements were carried out with an automated Risø TL/OSL-DA-20 system (Bøtter-Jensen et al., 2003), equipped with 28 blue LEDs (470 ± 20 nm) operating at 80% power (~40 mW cm^{-2}), and a $^{90}Sr/^{90}Y$ beta source, delivering ~0.11 Gy s^{-1}. Near UV emissions were measured through a Thorn EMI 9235 QA photomultiplier tube coupled with three Hoya U-340 detection filters, transmitting wavelengths between 290 and 370 nm. Photon emissions were detected for 60 s in 150 channels (bin width of 0.4 s), and the integral of the first 0.4 s minus the normalized integral from the last 20 s (background) was used for all luminescence intensity values. Heating for all preheat steps and luminescence measurements proceeded at a rate of 5 °C s^{-1}.

3. Refining a SAR TT-OSL protocol for dating loess

Aliquots were initially submitted to the simplified TT-OSL protocol of Stevens et al. (2009) (Table 1) because of the predictive power of the single transfer model for TT-OSL protocols applied to Chinese loess (cf. Pagonis et al., 2008). It has been suggested that the single transfer model implies the need for a 'TT-OSL-specific' test dose response, so the protocol measures the thermally-transferred test dose response. Additionally, the protocol incorporates a high temperature treatment (280 °C for 400 s) immediately following the TT-OSL ($L_{TT\text{-}OSL}$) measurement to prevent charge carry-over from the $L_{TT\text{-}OSL}$ measurement to the test dose ($T_{TT\text{-}OSL}$) measurement.

Apparent age underestimates and low signal-to-noise ratios were encountered when the Stevens et al. (2009) protocol was applied to the quartz grains from loess. Sample OTL 391, for example, had an average TT-OSL age of 123 ± 19 ka, compared with the IRSL age of ≥218.5 ± 17.9 ka, and an average signal-to-noise ratio of 2.56 ± 0.06 for the natural $L_{TT\text{-}OSL}$ and 2.16 ± 0.15 for the natural $T_{TT\text{-}OSL}$. Therefore, the protocol was modified to increase signal intensity: First, instead of a thermally-transferred test dose response, a test dose response was measured after a single preheat (T_{OSL}), under the assumptions that sensitization occurs at luminescence centers (Bailey, 2001) and that the fast component OSL traps and the TT-OSL source traps access the same luminescence centers (Adamiec et al., 2008; Pagonis et al., 2008). Second, the temperature of the T_{OSL} preheat (i.e., cutheat) was reduced to 220 °C to retain measurable emissions (Porat et al., 2009). Third, the final heat treatment was elevated to 350 °C for 200 s to minimize charge build-up with SAR cycling (Adamiec et al., 2010). Finally, the preheat temperatures were investigated to retain maximum ReOSL charge during the first preheat (Porat et al., 2009) and maximize the thermal transfer of TT-OSL charge during the second preheat (Fig. 1a in Tsukamoto et al., 2008).

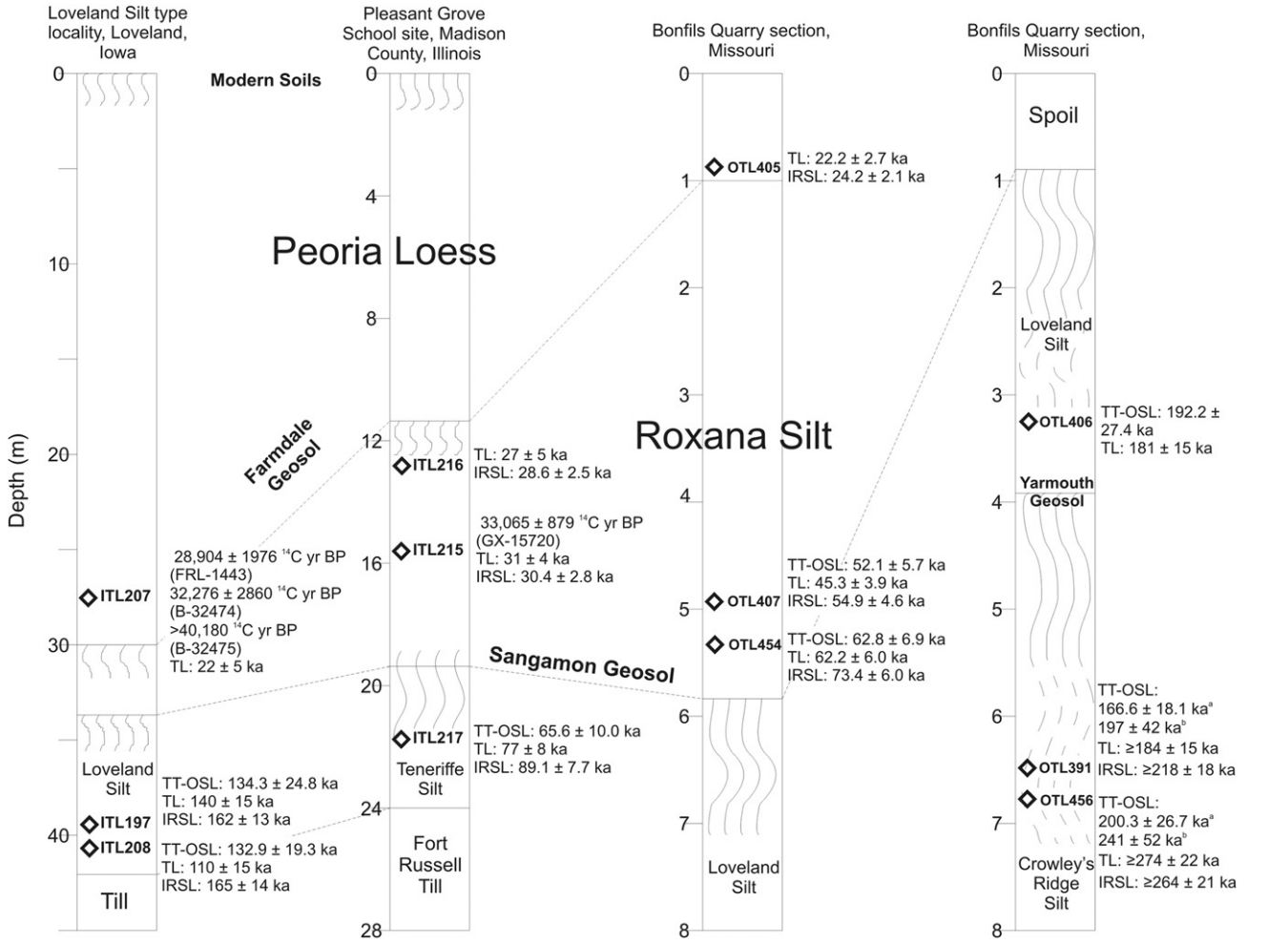

Fig. 1. Stratigraphic sequence and associated TL, IRSL, and radiocarbon ages for study sites. Radiocarbon ages are calibrated to calendar years before present using the calibration curve described in Fairbanks et al. (2005). Samples are identified adjacent to their location in the profile. Figure modified from Forman and Pierson (2002).

3.1. Equivalent dose plateaus with preheat temperatures

To isolate the effects of first- and second-preheat temperatures (Steps 2 and 4, Table 1), equivalent dose (D_e) values were measured for a single sample (ITL 197) using the protocol b from Table 1. Various temperatures for the 'first/second' preheats (°C) were tested: 180/260, 180/280, 180/290, 180/300, 180/310, 180/310; and 160/290, 180/290, 200/290, 220/290, 240/290. Samples were held at these temperatures for 10 s per preheat. Three aliquots were tested at each temperature combination. TT-OSL was measured at regeneration doses of 0, 151, 302, 605, and 151 Gy and the mean and standard deviation for D_e values are shown (Fig. 2). For the constant first preheat of 180 °C, the D_e values (Gy; $n = 3$) are listed according to their second-preheat temperatures (°C): 313.8 ± 30.9 (260), 416.8 ± 45.2 (280), 490 ± 70.0 (290), 450.0 ± 95.3 (300), 521.5 ± 50.0 (310); likewise for a constant second preheat of 290 °C and variable first preheats: 502.8 ± 18.9 (160), 490.0 ± 70.0 (180), 512.3 ± 88.1 (200), 606.8 ± 14.3 (220), 563.1 ± 49.6 (240).

The first preheat temperature was held constant at 180 °C, being <260 °C to avoid thermal depletion of the component of the TT-OSL signal that is sensitive to light (i.e., the recuperated OSL or 'ReOSL') (Porat et al., 2009), and >140 °C to evict thermally-unstable charge (Smith and Rhodes, 1994; Murray et al., 1997; Murray and Wintle, 2000). The D_e values increase and then plateau at a second-preheat temperature between 290 °C and 310 °C (Fig. 2b). The initial increase in D_e may imply that more charge is transferred from naturally-filled, thermally-shallow, and optically-insensitive traps (Murray and Wintle, 2000; Bailey, 2001). A plateau in D_e values suggests that the majority of the charge has been transferred, yielding maximum TT-OSL emissions. The second-preheat temperature was set at 290 °C because this is the D_e-plateau temperature furthest from the temperature of thermal eviction from the main OSL trap (325 °C) (Smith and Rhodes, 1994; Bailey et al., 1997). A plateau in D_e values is also observed with various temperatures for the first preheat (Fig. 2a), and 160 °C was chosen as the first preheat temperature due to the high precision in D_e values. Notably, the average D_e values for all aliquots from the first

Table 1
SAR TT-OSL protocols.

Step	Stevens et al. (2009)	Result	This study	Result
1	Dose, D_i	–	Dose, D_i	–
2	Preheat (260 °C, 10 s)	–	Preheat (160 °C, 10 s)	–
3	OSL (125 °C, 60 s)	–	OSL (125 °C, 60 s)	–
4	Preheat (260 °C, 10 s)	–	Preheat (290 °C, 10 s)	–
5	TT-OSL (125 °C, 60 s)	$L_{TT\text{-}OSL}$	TT-OSL (125 °C, 60 s)	$L_{TT\text{-}OSL}$
6	OSL (280 °C, 400 s)	–	OSL (280 °C, 400 s)	–
7	Test dose, D_t	–	Test dose, D_t	–
8	Preheat (260 °C, 10 s)	–	Preheat (220 °C, 10 s)	–
9	OSL (125 °C, 60 s)	–	OSL (125 °C, 60 s)	T_{OSL}
10	Preheat (260 °C, 10 s)	–	OSL (350 °C, 200 s)	–
11	TT-OSL (125 °C, 60 s)	$T_{TT\text{-}OSL}$		
12	OSL (290 °C, 400 s)	–		

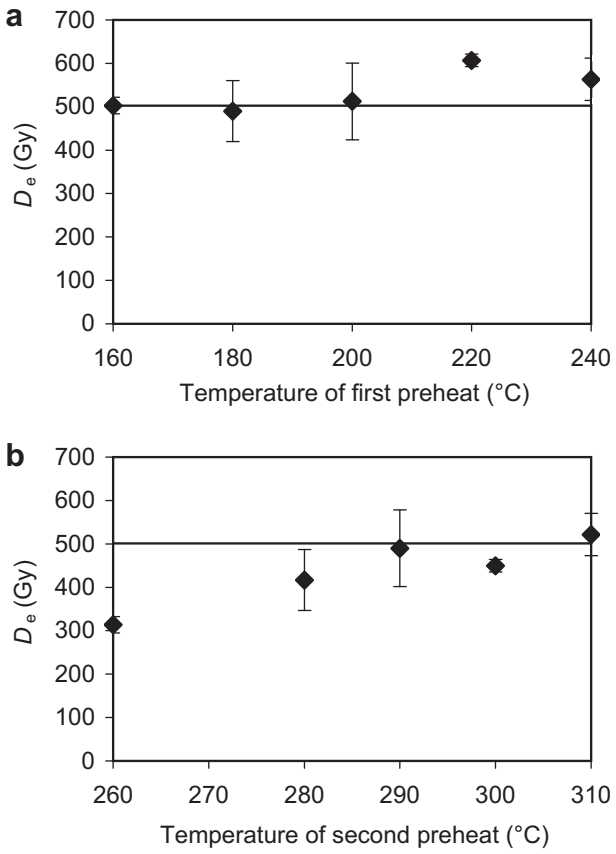

Fig. 2. Equivalent dose as a function of preheat temperatures for sample ITL 197. (a) The second-preheat temperature is kept constant at 290 °C. The regeneration doses are 0, 151, 302, 605, and 151 Gy, and the test dose is 67 Gy. Three discs are tested at each preheat temperature combination and the mean and standard error are displayed. The solid line marks the average D_e for first preheat temperatures 160–200 °C, which is 502.3 ± 17.9 Gy. (b) Same as in (a) for variations in second-preheat temperatures with first preheat temperature constant at 180 °C. The average D_e for preheat temperatures 290–310 °C is 501.4 ± 37.4 Gy. Note the similarity in the two plateau D_e values.

(160–200 °C) and second (290–310 °C) preheat plateau temperatures coincide at 1σ: 501.39 ± 37.44 Gy and 502.3 ± 17.9 Gy, respectively.

3.2. Test dose evaluation

For conventional SAR protocols, the luminescence resulting from the natural or regenerative irradiation (L) and the luminescence from the corresponding test dose irradiation (T) should relate linearly, and when plotted as a function of cycle ('L–T graph') the regression line should pass through the origin (Murray and Mejdahl, 1999; Wintle and Murray, 2006), although this requirement may be too restrictive for TT-OSL SAR protocols (Athanassas and Zacharias, 2010; Pagonis et al., 2011). Therefore, the relationship between $L_{TT\text{-}OSL}$ and T_{OSL} was monitored through repeated TT-OSL SAR measurement cycles for samples OTL 405 and OTL 454, with constant regeneration doses of 442 and 208 Gy and constant test doses of 44.2 and 20.8 Gy, respectively (Fig. 3).

Two conclusions are drawn from the L–T plot (Fig. 3). First, the relationship between $L_{TT\text{-}OSL}$ and T_{OSL} is linear ($R^2 > 0.95$ for both samples), which implies that increases in $L_{TT\text{-}OSL}$ sensitivity are accompanied by proportional increases in T_{OSL} sensitivity; this corroborates the idea that a common luminescence center is accessed and that the T_{OSL} signal is an appropriate measure of sensitivity change with TT-OSL SAR cycling (Porat et al., 2009).

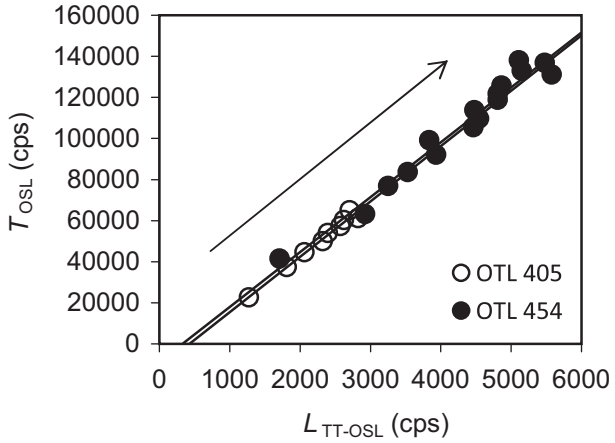

Fig. 3. TT-OSL signal ($L_{TT\text{-}OSL}$) as a function of the subsequent test dose OSL signal (T_{OSL}) with repeated TT-OSL SAR cycling for samples OTL 405 and OTL 454. The regenerative doses are similar to the previously estimated equivalent dose values (442 and 208 Gy for OTL 405 and 454, respectively) and the test doses are 10% of the regenerative doses. The arrow shows the direction of sensitivity change. Note the negative T-axis intercept.

Second, the regression lines do not intercept the origin. A corollary of this lack of direct proportionality at low $L_{TT\text{-}OSL}$ values is a 'lower limit' to TT-OSL accuracy; Fig. 3 implies that sensitivity changes cannot be monitored at very low $L_{TT\text{-}OSL}$ signals (e.g., <500 photons s^{-1}). This illustrates a critical limit to TT-OSL protocols, low signal magnitude (Stevens et al., 2009; Porat et al., 2009). This limitation should be considered when interpreting D_e estimates, particularly for samples with equivalent doses <200 Gy. However, many TT-OSL SAR studies report non-zero intercepts on L–T graphs despite successful dose recovery tests and favorable D_e comparisons with independent age estimates (Tsukamoto et al., 2008; Athanassas and Zacharias, 2010; Rosenberg et al., 2011). Moreover, recent numerical simulations of ReSAR protocols informed by a kinetic model of quartz (Bailey, 2001; Pagonis et al., 2008) produce L–T graphs wherein data points are linear but have significant non-zero T-axis intercepts; the accuracy and precision of these simulated protocols are not adversely affected (Pagonis et al., 2011). Therefore, the test dose magnitude (10% of expected D_e) appears to be an appropriate measure of sensitivity changes occurring during application of the TT-OSL SAR protocol. Further studies of TT-OSL sensitivity correction may be helpful, however, as a recent SAR OSL study indicates (Wang et al., 2012).

3.3. Dose response

The TT-OSL signal saturated at a higher dose than the fast OSL component, a phenomenon reported elsewhere (Wang et al., 2006; Rosenberg et al., 2011). The OSL and TT-OSL responses to regenerative doses can be fitted to the saturating exponential function,

$$I = I_o(1 - \exp[-D/D_o]) \quad (1)$$

where I is OSL intensity, D is the administered dose, I_o is the saturation intensity, and D_o is the dose characteristic of saturation. Wintle and Murray (2006) advise using $2D_o$ as the upper limit for D_e calculations. By this criterion, the OSL signal for OTL 456 is only valid to calculate D_e values <465.6 Gy (D_o = 232.8 Gy; Fig. 4a), and the expected D_e for OTL 456 is >862 Gy (Forman and Pierson, 2002). Hence, for OTL 456 conventional OSL measurements are inappropriate for D_e evaluation. Conversely, the TT-OSL dose–recovery curve is predicted to saturate at doses of ~2100 Gy (Fig. 4b), which validates the use of TT-OSL as a means to evaluate D_e for the oldest samples tested.

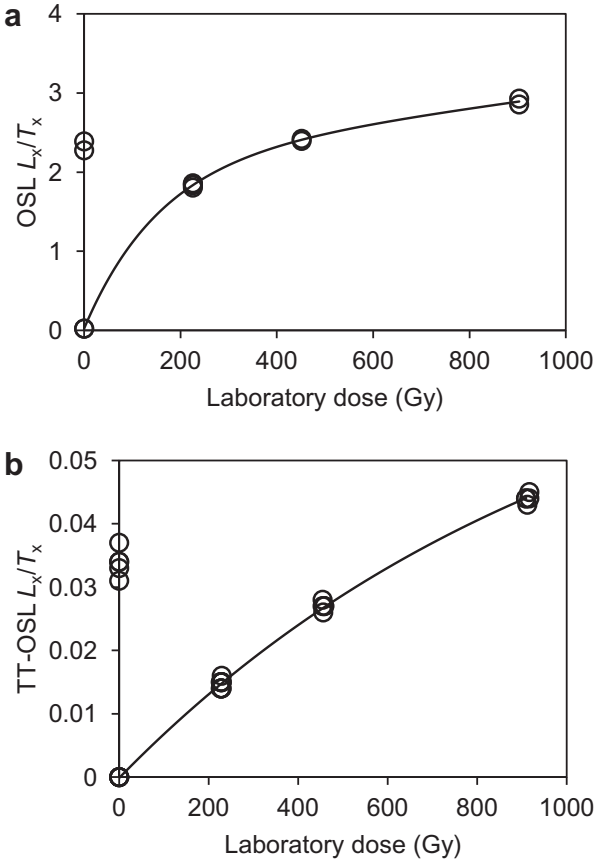

Fig. 4. Sensitivity-corrected OSL and TT-OSL response to laboratory dose for sample OTL 456. (a) OSL response to dose begins to saturate at higher doses and is unusable beyond ~466 Gy ($n = 2$), whereas (b) TT-OSL signal is far from saturation with beta irradiation doses up to 917 Gy ($n = 4$); the predicted upper limit for the TT-OSL best-fit line is ~2100 Gy.

4. Resetting the ReOSL signal

A prerequisite for the optical dating of mineral grains is that all charge accumulation prior to the most recent burial event must be reset by exposure to sunlight during pre-burial transportation (Aitken, 1998, pp. 143). Previous studies have demonstrated that the ReOSL signal diminishes more slowly than the fast component of the OSL signal when exposed to natural or pseudo-natural sunlight (Li et al., 2006; Tsukamoto et al., 2008; Kim et al., 2009). Quartz from Chinese loess and South African coastal sand retained 10–18% of the original ReOSL signal after a 7-day exposure to a SOL2 solar simulator (Tsukamoto et al., 2008), whereas another study of coastal terraces in southern Greece demonstrated a similar signal reduction in after only one-half hour of exposure to direct sunlight (Athanassas and Zacharias, 2010). A third study of dune and shallow marine quartz from South Africa estimated that 26 weeks of sunlight exposure would be needed to deplete the ReOSL signal to 1% (Jacobs et al., 2011).

To investigate the optical sensitivity of the thermally-transferred signal, sensitivity-corrected TT-OSL measurements (i.e., L_N/T_N; Steps 1–9, Table 1) were taken of samples OTL 391, OTL 454, and OTL 405 after various times of exposure to a General Electric 275-W mercury-vapor sunlamp. This lamp has continuous emissions in the visible light spectra and emits discrete wavelengths in the near UV region. Experiments on resetting of quartz luminescence indicate that 1 h sunlamp exposure is approximately equal to ~1.2 h of sunlight. These samples vary significantly in IRSL D_e, with values of 695.7 ± 9.2 Gy (OTL 391), 241.8 ± 1.9 Gy (OTL 454), and 82.7 ± 2.9 Gy (OTL 405). TT-OSL intensities were measured after 0, 0.01, 0.1, 1 8, 48, and 95 h of exposure to the sunlamp. Three aliquots per sample were measured for each exposure time. All three samples exhibited a logarithmic decay in TT-OSL with exposure time; however, none of the samples were optically reset to a negligible level (Fig. 5). After 1 h of sunlamp exposure, samples retained 86.1 ± 8.4% (OTL 391), 75.8 ± 58.8% (OTL 405), and 91.1 ± 9.5% (OTL 454) of the initial, natural TT-OSL intensity, and even after 95 h of sunlamp exposure, 40.2 ± 4.3% (OTL 391), 27.1 ± 12.8% (OTL 405), and 49.8 ± 34.4% (OTL 454) of the natural signal remained. To reset the signal to 1% could require months of sunlight exposure, though effects such as high altitude could reduce this time.

5. Dose recovery test

Considering the persistence of the ReOSL signal, young-to-modern samples should be used for TT-OSL dose recovery tests to ensure that the ReOSL traps are completely emptied prior to laboratory irradiation (Adamiec et al., 2010). Alternately, the natural (Tsukamoto et al., 2008) or post-bleach (Kim et al., 2009) D_e value may be subtracted from the recovered dose when evaluating TT-OSL dose recovery tests. As no modern (i.e., naturally zeroed) samples exist within the suite of samples, the dose recovery test was performed using both suggested methods: a) to optically zero, then irradiate a sample (OTL 405), and b) to (additively) irradiate a sample with a well-known age (ITL 207).

First, the youngest sample available was tested for dose recovery. OTL 405 from the Peoria Loess is estimated to have a D_e of 75 ± 8 Gy (TL) and 83 ± 3 Gy (IRSL) (Forman and Pierson, 2002). After 48 h of exposure to a sunlamp, three aliquots of sample OTL 405 were given a beta dose of 500 Gy, and the average recovered dose was 485 ± 34 Gy (Fig. 6). From the UV lamp exposure tests in the previous section, the natural $L_{TT\text{-}OSL}/T_{OSL}$ value remaining for OTL 405 after 48 h exposure to the sunlamp was 0.0023 ± 0.0017 ($n = 3$), and the value measured without lamp exposure was 0.033 ± 0.001 ($n = 3$); this comparison implies that the error associated with post-bleach charge should be <10% of the natural signal. The average recycling ratio for these aliquots was 0.87 ± 0.07, which falls slightly outside of the optimal range of 1.0 ± 0.1; the effect appears to be minimal with regard to D_e estimation and may reflect minor build-up from the TT-OSL source traps which are insensitive to sunlight (basic transferred

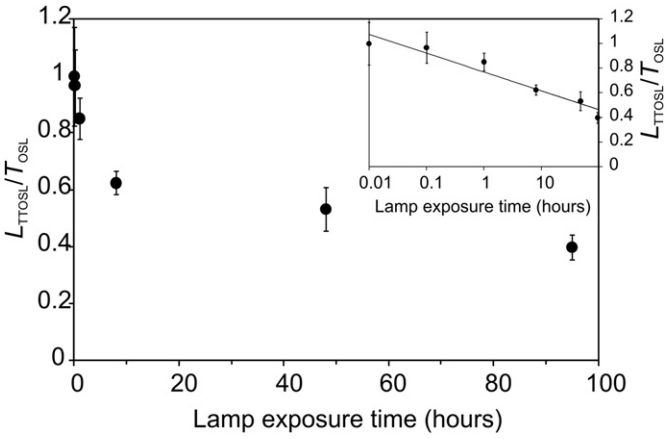

Fig. 5. Sensitivity-corrected TT-OSL intensity remaining after various sunlamp exposure times for sample OTL 391. Each point represents the average measurement from three aliquots and the associated 1σ error, normalized to the pre-exposure luminescence intensity. The inset shows the same data with time on a logarithmic axis.

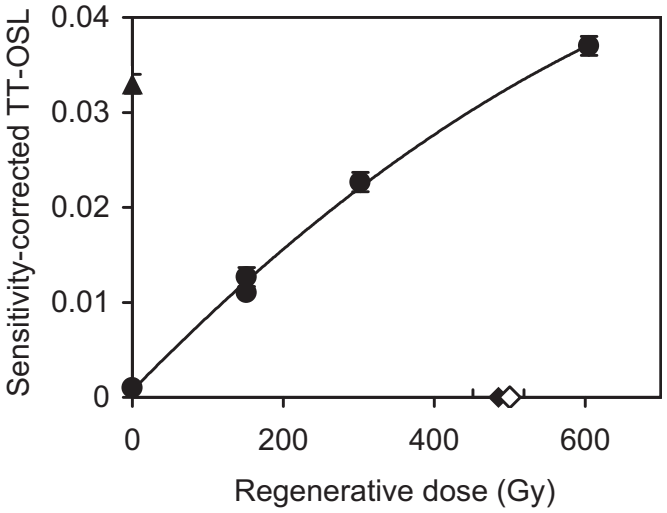

Fig. 6. The dose recovery test for sample OTL 405 measured with the protocol shown in Table 1. The closed triangle is the 'natural' signal, the closed diamond is the corresponding equivalent dose of 485 ± 34 Gy, and the open diamond is the given dose of 500 Gy. Data are averaged from three aliquots and a saturating exponential is fitted to the regenerative dose response points.

OSL, or 'BT-OSL'), or a differential sensitivity change between $L_{TT\text{-}OSL}$ and T_{OSL} measurements (Wintle and Murray, 2006; Stevens et al., 2009).

Second, a well-constrained sample was tested for dose recovery. Sample ITL 207, also from the Peoria Loess, has previously been dated with IRSL methods ($D_e = 81.9 \pm 0.3$ Gy; Forman and Pierson, 2002), and therefore dose recovery can be monitored by accounting for both burial dose and beta dose administered. Three aliquots of ITL 207 were exposed to 800 Gy of beta irradiation, which is added to the inherent ~82 Gy to give a total expected dose of 881.9 ± 0.3 Gy. This method circumvents uncertainty associated with incomplete resetting of the TT-OSL signal. The recovered dose for these three aliquots was 875 ± 41 Gy, a 1σ correspondence with the expected dose. All three discs showed a zero-dose response of nearly 10% of the natural signal, though this is attributed to the low magnitude of the TT-OSL regenerative signal rather than charge build-up.

6. Isothermal decay analysis

The thermal stability of the TT-OSL source traps is a key concern to avoid underestimates of burial dose (Adamiec et al., 2010; Pagonis et al., 2011). Therefore, isothermal decay analysis was performed to investigate the thermal stability of the ReOSL trap (cf., Spooner and Questiaux, 2000), using the LM-OSL signal isolation method (Singarayer, 2002). An aliquot of OTL 391 was first heated (350 °C, 200 s) under blue-light stimulation to clear the TT-OSL signal. Next, the sample received a beta irradiation of ~329 Gy. The sample then experienced the first three steps of the TT-OSL protocol (preheat, OSL, preheat; Table 1). At this stage in a typical TT-OSL protocol, the TT-OSL signal would be measured; instead, the sample was held at temperature T °C for t seconds. Temperatures and hold-times are shown in Table 2. Following the respective heat treatment, the thermally-transferred LM-OSL signal was measured for 400 s at 160 °C. The LM-OSL response to a test dose of 110 Gy (followed by a cutheat of 220 °C for 10 s) was measured at the end of each sequence. This sequence was repeated for every combination of time and temperature shown in Table 2. The LM-OSL signals measured were then analytically separated into three components of the form

Table 2
Heat treatments used in isothermal decay analysis.

T (°C)	270	290	310	330	350
Time (s) held at temperature	0	0	0	0	0
	70	40	10	10	10
	250	80	40	40	40
	600	150	100	100	100

$$I(t) = n_o\left(\sigma P t^2/T\right)\exp\left(sPt^2/T\right) \quad (2)$$

where $I(t)$ is the LM-OSL intensity (cps) at time t (s), n_o is proportional to the initial trapped charge concentration, σ is the photoionization cross-section (cm^2), P is the maximum stimulation intensity (mW cm^{-2}), and T is the total stimulation time (s) (Singarayer and Bailey, 2003). Each of the three LM-OSL components represents the contribution of charge from an individual trap (fast, medium, slow); the fast trap component is identified by rapid optical depletion (i.e., greatest value of σ) (Jain et al., 2003). The ReOSL and BT-OSL traps both empty into the fast component trap during thermal transfer (Pagonis et al., 2008), and assuming the majority of the transferred charge is from the ReOSL trap (Kim et al., 2009 indicates that ~97% of the total TT-OSL signal is derived from the ReOSL traps), the isothermal decay of the fast component of the 'TT-LM-OSL' signal should approximate the isothermal decay of the ReOSL traps. Therefore, the n_o best-fit parameter (proportional to trapped charge) from Equation (2) was found for each post-heat treatment LM-OSL measurement using least-squares analysis within LAB Fit Curve Fitting Software, version 7.2.43 (http://www.labfit.net). For each heat temperature, n_o values were plotted according to the time held at that temperature to find the isothermal decay constant, τ. Finally, an Arrhenius plot was constructed by plotting $\ln(\tau)$ (s) on the y-axis and $1/T$ (°K) on the x-axis (Fig. 7). The ReOSL trap parameters of trap depth, E (eV), and trap frequency factor, s (s^{-1}), can be extracted from the Arrhenius plot by assuming that a best-fit line describes the following relationship:

$$\ln(\tau) = \ln\left(s^{-1}\right) + (E/\kappa_B)(1/T) \quad (3)$$

where τ is the isothermal decay constant at temperature T (°K), s is the frequency factor (s^{-1}), E is the trap depth (eV), and κ_B is Boltzmann's constant (~8.615×10^{-5} eV K^{-1}) (Singarayer, 2002).

This method yields ReOSL trap parameter values of $E = 1.57$ eV and $s = 3.1 \times 10^{11}$ s^{-1}. These values compare with previously

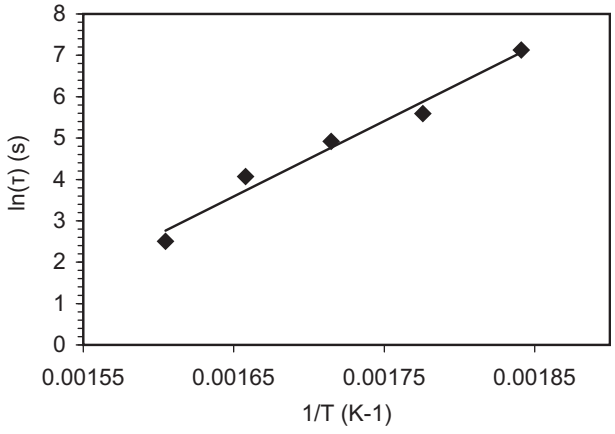

Fig. 7. Arrhenius plot of the natural log of the isothermal decay constant (y-axis) plotted against the inverse of the hold temperature. ReOSL trap depth (E) is derived from the slope of the best-fit line and the ReOSL trap frequency factor (s) is derived from the y-intercept value (cf. Singarayer, 2002).

published values: Pagonis et al. (2008) used E and s values of 1.65 eV and 6.5×10^{13} s^{-1} for numerical simulations of the ReOSL trap based on observations of the 325 °C TL peak in Spooner and Questiaux (2000). These parameter values simulated the ReOSL signal well, but a robust simulation of empirical data does not preclude different trap parameter values (Pagonis et al., 2008). Adamiec et al. (2010) investigated ReOSL trap parameters by measuring TL glow curves before and after various optical stimulation and heating routines. 1.46 eV and 7.60×10^{11} s^{-1} were estimated as the ReOSL trap E and s values based upon the TL peak positions (Adamiec et al., 2010). The isothermal decay E value for this study is similar to the previous studies; however, the isothermal decay s value appears to favor the Adamiec et al. (2010) empirical TL peak s value instead of the inferred value used in the Pagonis et al. (2008) numerical simulations. It is recognized that errors are introduced into E and s calculations during all three data fitting steps, and the degree of final error is uncertain (Singarayer, 2002). Trap lifetime estimations using isothermal decay analysis also assumes that the eviction processes are simple (i.e., first order) and that it is valid to extrapolate from laboratory- to actual-decay times (Aitken, 1998, pp. 200).

The thermal lifetime of trapped charge can be estimated from the ReOSL trap parameters, E and s. However, trap thermal stability has a strong dependence on the burial temperature, so the temperature during the burial period is required for this calculation (Aitken, 1998, pp. 201). For example, according to the calculated E and s values, the ReOSL trap has a lifetime of 9065, 861, or 96 Ma at burial temperatures of 0, 10, or 20 °C, respectively. The mean integrated temperature during the burial of the Crowley's Ridge Silt at the Bonfils Quarry location was investigated because the oldest samples would experience the most thermal decay with time. Epimerization of isoleucine in subfossil gastropod shells from Peoria Loess of the Mississippi Valley implies a mean annual ground temperature of ~8 °C at the latitude and depths of interest for the past 20 ka (Oches et al., 1996). $\delta^{18}O$ data from speleothems in Missouri offer insight into the period of ~25–75 ka (Dorale et al., 1998). During this period the mean annual temperature of the surface atmosphere varied within a range of ~4 °C (Dorale et al., 1998). A climate model simulation offers insight into MIS Stage 5e, the last full interglacial, which appears to have been ~4 °C warmer than present (Crowley and Kim, 1994). Finally, ostracod assemblages and pollen records from glacial lake sediments in western Tennessee suggest that the regional temperature regime during MIS 6 was comparable to that of the Wisconsinan glacial period (Grimley et al., 2009). As a time-weighted average, these data suggest a mean burial temperature of about ~10 °C during the period of ~0–190 ka, assuming a modern mean annual air temperature of ~14 °C for the Bonfils Quarry region (Oches et al., 1996).

Assuming a mean burial temperature of ~10 °C, the ReOSL trap is expected to have a lifetime of 943 Ma. Aitken (1998, pp. 200) advises using traps with lifetimes ten times larger than the expected burial dose to avoid systematic underestimation of more than 5%. By this criterion the ReOSL trap appears stable enough to date samples from the Late Pleistocene. However, the errors incurred during the calculation of E and s should be considered. For example, the slope of the best-fit line in Fig. 7 is $(1.57 \pm 0.14)/\kappa_B$, which means that the 1σ lower limit for the trap depth, E, results in a trap lifetime of 3 Ma. Likewise, the 1σ upper limit for the frequency factor, s, yields a trap lifetime of 57 Ma. A combination of both the lower limit E and the upper limit s gives a trap lifetime of 162 ka. We consider the final case unlikely and assume sufficient thermal stability for the oldest samples.

7. TT-OSL ages

The TT-OSL SAR protocol was applied to all five loess units and 114 aliquots were analyzed. Dose–response curves were constructed for each aliquot using five regeneration-dose responses. Aliquots were rejected if the zero-dose response was >5% of the sensitivity-corrected natural signal, or if the recycling ratio was beyond 10% of unity (Murray and Wintle, 2000). This protocol is time-consuming. For example, the oldest samples require 8 h per aliquot to produce a single regenerative dose curve. Constructing a standardized growth curve with a few aliquots and measuring only the natural signal for the remaining aliquots may be a more efficient approach (Roberts and Duller, 2004; Kim et al., 2009, 2010).

All TT-OSL equivalent doses and calculated ages are shown in Table 3, along with the previously calculated IRSL and TL values (Forman et al., 1992; Forman and Pierson, 2002). Equivalent dose values are calculated using aliquots with acceptable recycling ratios (0.9–1.10) and zero-dose responses of <5% L_N/T_N; ~40% of aliquots

Table 3
TL, IRSL, and TT-OSL dose-rate data and ages for midcontinental United States loess deposits.[a]

Sample number	Th (ppm)	U (ppm)	K_2O (%)	TT-OSL dose rate (mGy/yr)	TT-OSL D_e (Gy)	TT-OSL age (ka)	IRSL D_e (Gy)	IRSL age (ka)	TL D_e (Gy)	TL age (ka)	TT-OSL aliquots (#used/#tested)
Peoria Loess											
ITL 207	6.74 ± 0.97	3.32 ± 0.30	2.25 ± 0.04	3.89 ± 0.14	N/A	N/A	81.9 ± 0.3	24.4 ± 1.9	88.0 ± 11.7	22 ± 3	0/6
OTL 405	6.51 ± 0.91	2.88 ± 0.36	2.24 ± 0.02	3.32 ± 0.15	N/A	N/A	82.7 ± 2.9	24.2 ± 2.1	74.9 ± 7.6	22.2 ± 2.7	0/6
Roxana Silt											
ITL 215	5.83 ± 0.85	2.09 ± 0.26	2.27 ± 0.04	3.02 ± 0.12	N/A	N/A	82.2 ± 3.5	30.4 ± 2.8	101.2 ± 15.4	31 ± 4	0/6
ITL 216	4.48 ± 0.75	2.22 ± 0.24	1.89 ± 0.04	2.65 ± 0.11	N/A	N/A	86.5 ± 2.7	28.6 ± 2.5	82.2 ± 15.7	27 ± 5	0/6
OTL 407	7.90 ± 1.19	2.70 ± 0.43	2.12 ± 0.02	3.31 ± 0.18	172.6 ± 6.1	52.1 ± 5.7	182.6 ± 3.5	54.9 ± 4.6	199.3 ± 11.3	45.3 ± 3.9	1/10
OTL 454	7.29 ± 1.11	3.19 ± 0.42	1.99 ± 0.02	3.32 ± 0.17	208.3 ± 8.0	62.8 ± 6.9	241.8 ± 1.9	73.4 ± 6.0	214.6 ± 2.9	62.2 ± 6.0	4/6
Teneriffe Silt											
ITL 217	5.32 ± 0.64	2.08 ± 0.20	1.84 ± 0.04	2.65 ± 0.09	173.9 ± 24.8	65.6 ± 10.0	245.4 ± 1.9	89.1 ± 7.7	202.3 ± 19.6	77 ± 8	8/15
Loveland Silt											
ITL 197	7.08 ± 0.97	2.37 ± 0.30	2.22 ± 0.05	3.19 ± 0.14	429.0 ± 80.2	134.3 ± 24.8	511.6 ± 2.9	161.6 ± 13.4	644.0 ± 69.3	140 ± 15	5/6
ITL 208	6.94 ± 0.96	2.51 ± 0.30	2.18 ± 0.04	3.20 ± 0.14	425.3 ± 54.7	132.9 ± 19.3	512.5 ± 3.9	165.0 ± 14.5	389 ± 47.8	110 ± 15	6/12
OTL 406	8.28 ± 1.14	2.58 ± 0.42	1.90 ± 0.02	3.15 ± 0.18	605.2 ± 71.0	192.2 ± 27.4	599.1 ± 6.2	182.0 ± 14.6	643.5 ± 19.6	181.5 ± 15.1	4/16
Crowley's Ridge Silt											
OTL 391	9.20 ± 1.25	2.33 ± 0.37	1.95 ± 0.02	3.19 ± 0.19	532.0 ± 18.8	166.6 ± 18.1	695.7 ± 9.2	≥218.5 ± 17.9	581.6 ± 8.5	≥183.8 ± 15.0	11/13
OTL 456	8.66 ± 1.18	2.11 ± 0.42	1.90 ± 0.02	3.03 ± 0.18	607.1 ± 58.7	200.3 ± 26.7	861.3 ± 9.1	≥264.5 ± 21.1	877.7 ± 12.1	≥274.4 ± 22.2	6/12

[a] All data are shown with 1σ error; TT-OSL ages are calculated using the central age model of Galbraith et al. (1999); all measurements except for the TT-OSL dose-rates, ages, and equivalent doses were previously published in Forman et al. (1992) and Forman and Pierson (2002).

satisfy these criteria. Age uncertainties are calculated by incorporating uncertainties associated with dose rate and equivalent dose estimates into a variance–covariance matrix (Marquardt, 1963). Importantly, there is 1σ agreement between TT-OSL ages and published TL and IRSL ages, with the notable exception of the Crowley's Ridge Silt, for which there is 2σ agreement between TT-OSL and TL or IRSL ages. Caution should be exercised when interpreting comparisons between TL, IRSL, and TT-OSL D_e estimates, as the TL and IRSL ages for the Crowley's Ridge Silt samples (OTL 391 and OTL 456) are neither finite nor reliable (Forman and Pierson, 2002). The reason for this uncertainty is saturating signal growth with irradiation, which leads to large uncertainties when extrapolating to find the equivalent dose and, transitively, the age (Wintle and Huntley, 1982). Therefore, for the Crowley's Ridge Silt, the TT-OSL ages should not be dismissed simply because they are younger than the IRSL and TL ages.

Difficulties are encountered when the youngest loess units (IRSL $D_e < 200$ Gy; Forman and Pierson, 2002) are evaluated. Samples from the Peoria Loess and Roxana Silt with IRSL $D_e < 200$ Gy exhibited recycling ratios and recuperation levels beyond the allowable limits. The mean recycling ratios and recuperation values (% of L_N/T_N) for all aliquots with IRSL $D_e < 200$ Gy are 0.96 ± 0.32 and $11.7 \pm 13.3\%$, respectively ($n = 34$). By comparison, aliquots with IRSL $D_e > 200$ Gy have values of 0.95 ± 0.10 and $1.2 \pm 1.7\%$ ($n = 80$). This suggests that ~200 Gy may be the lower limit of recoverable D_e values when using TT-OSL on quartz from loess deposits in the midcontinental United States. This limit reflects low TT-OSL signal intensity, an effect which is most pronounced in sediments younger than ~50 ka.

8. Discussion

The fast component of the measured TT-OSL signal may need to be isolated, assuming that the ReOSL traps empty into the fast component OSL traps during the thermal transfer heating (Pagonis et al., 2008). A plot showing D_e values calculated using fixed bin-width integration limits at various times after stimulation begins ('$D_e(t)$-plot'; Bailey, 2000) is useful to test for this effect. If the fast component is dominant, the D_e value should be the same at every integration interval. However, if the TT-OSL signal yields different D_e values at different integration intervals, the medium and slow components may be contaminating the TT-OSL signal and the fast component should be isolated to avoid age underestimates. For example, Tsukamoto et al. (2008) observed a trend of increasing TT-OSL D_e underestimations with larger doses when performing dose recovery tests. To overcome this effect, the empirical TT-OSL signal was mathematically separated into fast, medium, and slow components and a constant. The equivalent dose was then calculated using only the fast component of the TT-OSL signal. In their study, the ratios of recovered-to-given laboratory doses were near unity for all doses when the fast component TT-OSL signal was analyzed, suggesting that such a separation may be necessary for accurate dose recovery (Tsukamoto et al., 2008). Therefore, for the present study, equivalent dose values are evaluated at various integration times and for the fast component individually.

8.1. Equivalent dose by integration time

$D_e(t)$-plots were constructed to check for variations in D_e by signal components (Fig. 8b). For the three samples examined (two from Crowley's Ridge Silt and one from the Roxana Silt) D_e values decrease supralinearly for integration times of 0.4–2 s before reaching a reaching plateaus. This suggests that using the first 0.4 s of TT-OSL signals to calculate D_e values (i.e., TT-OSL D_e values in Table 3) inadvertently incorporates multiple components with different dose response characteristics and therefore probably provides minimum age estimates.

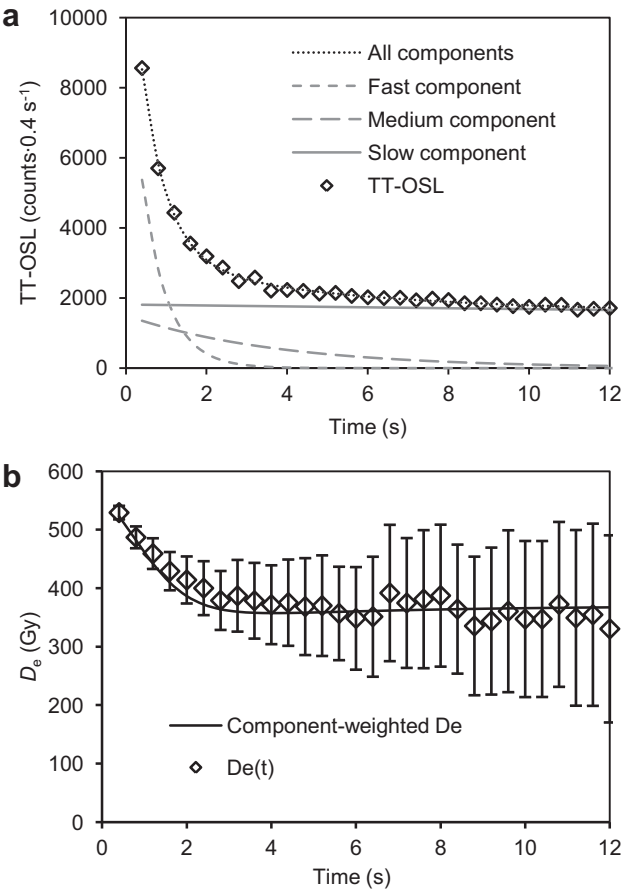

Fig. 8. Signal components and $D_e(t)$-plot for sample OTL 391. (a) A linear combination of three exponential components fitted to the natural TT-OSL of a single aliquot. (b) Diamonds represent the average D_e values for all aliquots when integrated using the TT-OSL curves at time t (i.e., $D_e(t)$-plot). The natural and regenerative curves are fitted to a linear combination of three exponential decay functions (fast, medium, and slow), and D_e is estimated using the dose–response curves from these individual components. The $D_e(t)$-plot is then recreated assuming the D_e at any instant is the linear combination of all three component-specific D_e's weighted by the relative proportion of signal contribution (solid black curve).

To further investigate the importance of separating the fast component from the TT-OSL signal, the natural and regenerative $L_{TT\text{-}OSL}$ and T_{OSL} signals from a single aliquot of OTL 391 were fitted to a linear combination of three exponential functions

$$I = a \cdot \exp(-b \cdot t) + c \cdot \exp(-d \cdot t) + e \cdot \exp(-f \cdot t) \quad (4)$$

where I is TT-OSL intensity (cps), t is time (s), and a–f are constants estimated using a Levenberg–Marquardt least-squares algorithm (Marquardt, 1963) within LAB Fit Curve Fitting Software (Fig. 8a). D_e values were calculated using only the best-fit components termed 'fast', 'medium', and 'slow' for discussion purposes, although the photoionization cross-sections were not calculated (e.g., Bailey et al., 1997; Jain et al., 2003). Finally, the natural $L_{TT\text{-}OSL}$ signal was deconvoluted into the three exponential decay components and a 'pseudo-$D_e(t)$' function was calculated as the linear combination of the component-specific D_e values weighted by the relative proportion of the components at various times. For example, if at $t = 1.2$ s there is 75% fast component, 20% medium component, and 5% slow component contribution, and D_e (fast) = 700 Gy, D_e (medium) = 600 Gy, and D_e (slow) = 500 Gy, then the pseudo-$D_e(t)$ equation would be

$$\text{pseudo} - D_e(1.2\text{ s}) = (0.75 \cdot 700\text{ Gy}) + (0.2 \cdot 600\text{ Gy}) + (0.05 \cdot 500\text{ Gy}) \quad (5)$$

The pseudo-$D_e(t)$ is shown in Fig. 8a as a solid black curve. The 1σ correspondence between the pseudo- and empirical-$D_e(t)$ data implies that the empirical $D_e(t)$ represents a linear combination of component-specific D_e values and not a single TT-OSL source trap D_e value. This observation corroborates the mechanism of thermal transfer into the fast component OSL trap. Only the fast component trap should donate TT-OSL charge to the luminescence center and therefore contribution from the medium and slow components should obscure the true TT-OSL equivalent dose. Therefore, the fast component D_e should be isolated for accurate paleodose recovery.

8.2. Natural-to-regenerative TT-OSL ratio

Further complications are encountered when the fast component is proportionally more dominant in the natural than the regenerative TT-OSL signals. Steffen et al. (2009) isolated this effect using the ratio of the natural-to-regenerative OSL signals according to integration time (i.e., an NR(t) plot). Ratios below 1 indicate that the fast component is present in a lesser proportion for regeneration dose TT-OSL signals and that the medium and slow components are correspondently larger (Steffen et al., 2009). Interestingly, aliquots with a negative slope on NR(t) plots have also been observed to produce a negative slope on $D_e(t)$ plots (Steffen et al., 2009), a phenomenon also observed in the present study. The NR(t) and $D_e(t)$ plots for the same aliquot of sample OTL 456 are shown in Fig. 9. For aliquots with decreasing values for both N/R and D_e with integration time, Steffen et al. (2009) obtained higher D_e values when using only the fast component for D_e calculation. To estimate fast component D_e values for our study, CW-OSL curves were mathematically deconvoluted to isolate the fast component contribution for the conventional OSL signals. Unfortunately, the low magnitude of the TT-OSL signal makes such deconvolutions (Fig. 8a) subjective and imprecise.

Moreover, the NR(t) plot suggests a possible reason for the success of the dose recovery test despite age imprecision for the oldest samples. The natural signal decays more quickly than the regenerative signal, which implies that the TT-OSL source traps fill differently in nature than in the laboratory. The fast component may be more dominant in the natural signal because irradiations taking place over thousands of years allow for thermally-unstable charge to transfer to the TT-OSL source traps. To test this hypothesis, the ratio of a sensitivity-corrected natural TT-OSL (OTL 456) to the sensitivity-corrected pseudo-natural TT-OSL (ITL 207 + 800 Gy) was plotted by integration time. The ratio was found to decrease with time, suggesting that even for comparable dose amounts (~880 Gy), the fast component traps for the TT-OSL natural and pseudo-natural are populated in different proportions. Therefore, a dose recovery test may show a 'given/recovered' dose ratio near unity because trap filling is similar in the pseudo-natural irradiation and the regenerative irradiations. However, the trap filling which occurs naturally will be different than trap filling in response to laboratory regenerative doses, which will lead to inaccurate estimations of the natural dose if a simple integration technique is used instead of fast component separation.

These observations imply the need to extract the fast component from the bulk TT-OSL signal, either by analytical separation or direct measurement. Unfortunately, it is difficult to directly measure the fast component. LM-OSL measurements provide more distinct component signals, but curve deconvolutions are still required and high signal intensity is a prerequisite (cf. Jain et al., 2003). Similarly, stimulating samples with IR light at elevated temperatures depletes the fast component only, allowing for a protocol based on the difference between pre- and post-IR OSL measurements ('differential-OSL'; Jain et al., 2005). However, this differential-OSL measurement also requires sufficient signal strength (Steffen et al., 2009). The accuracies of some TT-OSL dose recovery tests have been improved by deconvoluting the fast component from CW-OSL measurements, and then estimating D_e values using only the fast component (Tsukamoto et al., 2008). Therefore, for this study D_e values were estimated using the fast component deconvoluted from the total CW-OSL signal. The fast component D_e values were indeed higher than the bulk signal TT-OSL D_e values. The preliminary ages based on fast component TT-OSL are 241 ± 52 ka for OTL 456 (n = 1) (TT-OSL age of 200.3 ± 26.7 ka), and 197 ± 42 ka for OTL 391 (n = 1) (TT-OSL age of 166.6 ± 18.1). The fast component TT-OSL ages should be more accurate (Tsukamoto et al., 2008), but given current analytical and instrumental component separation methods, an efficient and precise protocol remains elusive. The future development of the TT-OSL chronology for the midcontinental US loess sheets may therefore hinge on the ability to efficiently separate the fast component from the bulk TT-OSL signal.

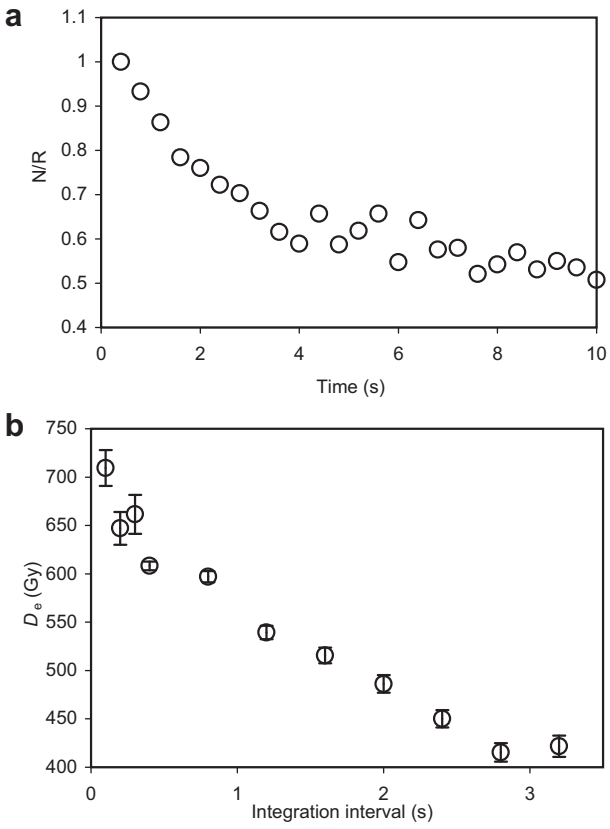

Fig. 9. NR(t) and $D_e(t)$ plot for sample OTL 456. (a) Natural-to-regenerative TT-OSL ratios (N/R) by integration time. The decreasing ratio with increasing time implies that the regenerative TT-OSL signal has proportionately less fast component contribution. (b) D_e values by integration. The negative slope suggests that the fast component retains a higher D_e value than the bulk (TT-)OSL signal.

9. Conclusions

Fine-grained quartz extracts from loess deposits in the midcontinental United States were submitted to a modified SAR TT-OSL protocol (Table 1, Stevens et al., 2009) to refine the loess depositional chronology. The modified protocol achieved adequate recycling ratios, negligible zero-dose luminescence response, and dose

recoveries near unity. When tested on samples, the protocol produced TT-OSL signal growth at doses up to ~917 Gy. The protocol was used to calculate equivalent doses and apparent ages for the Roxana Silt, Loveland Silt, Teneriffe Silt, and Crowley's Ridge Silt. Ages for the Roxana Silt (~52–63 ka), Teneriffe Silt (~66 ka), and Loveland Silt (~133–192 ka) agree at 1σ with previously published TL and IRSL ages. For samples with $D_e >$ ~400 Gy TT-OSL fast component D_e values are favored and avoid the problem of quartz OSL dose saturation.

The TT-OSL signal may be contaminated by the medium and slow components if the fast component is not dominant during optical stimulation. Unless these contaminating components are separated, either by differentially stimulating the fast component, or by mathematically separating the respective curves, the apparent TT-OSL age will be mixed with the medium and slow component apparent ages. Moreover, the difference in signal decay between the natural and regenerative TT-OSL signals suggests that trap filling in nature is different than trap filling in the laboratory (Fig. 9a). This would explain the accurate dose recovery tests, with no discrepancy between the pseudo-natural and the regenerative trap filling.

In the present study, fast component separation was attempted analytically by curve deconvolution, assuming three components. Unfortunately, this method is time-consuming and subjective, i.e., the chosen initial conditions for least-squares analyses bias the best-fit results when deconvoluting the TT-OSL signal. The resolved fast component TT-OSL ages were older than the bulk signal TT-OSL ages and appear to support either a marine oxygen-isotope stage (MIS) 7 (~191–243 ka; Lisiecki and Raymo, 2005) or MIS 8 (~243–300 ka) deposition (197 ± 42 and 241 ± 52 ka for samples OTL 391 and 456, respectively), contrary to the MIS 12 interpretation (Grimley et al., 2003).

Acknowledgments

This manuscript has been significantly improved thanks to comments from Grzegorz Adamiec, Xulong Wang, and Frank Preusser. We thank Jeaneth Mazzocco and James Pierson for their expert assistance in sample preparation and analysis. This work was supported by the National Science Foundation Award EAR-0602308.

Editorial handling by: F. Preusser

References

Adamiec, G., Aitken, M., 1998. Dose rate conversion factors: update. Ancient TL 16, 37–50.

Adamiec, G., Bailey, R.M., Wang, X.L., Wintle, A.G., 2008. The mechanism of thermally transferred optically stimulated luminescence in quartz. Journal of Physics D: Applied Physics 41, 135503.

Adamiec, G., Duller, G.A.T., Roberts, H.M., Wintle, A.G., 2010. Improving the TT-OSL SAR protocol through source trap characterization. Radiation Measurements 45, 768–777.

Aitken, M.J., 1998. An Introduction to Optical Dating. Oxford University Press, Oxford, 267 pp.

Athanassas, C., Zacharias, N., 2010. Recuperated-OSL dating of quartz from Aegean (South Greece) raised Pleistocene marine sediments: current results. Quaternary Geochronology 5, 65–75.

Bailey, R.M., 2000. The interpretation of quartz optically stimulated luminescence equivalent dose versus time plots. Radiation Measurements 32, 129–140.

Bailey, R.M., 2001. Towards a general kinetic model for optically and thermally stimulated luminescence of quartz. Radiation Measurements 33, 17–45.

Bailey, R.M., Smith, B.W., Rhodes, E.J., 1997. Partial bleaching and the decay form characteristics of quartz OSL. Radiation Measurements 27, 123–136.

Begét, J.E., 2001. Continuous Late Quaternary proxy climate records from loess in Beringia. Quaternary Science Reviews 20, 499–507.

Bettis, E.A., Muhs, D.R., Roberts, H.M., Wintle, A.G., 2003. Last Glacial loess in the conterminous USA. Quaternary Science Reviews 22, 1907–1946.

Berger, G.W., Mulhern, P.J., Huntley, D.J., 1980. Isolation of silt-sized quartz from sediments. Ancient TL 18, 7–11.

Blum, M.D., Guccione, M.J., Wysocki, D.A., Robnett, P.C., Rutledge, E.M., 2000. Late Pleistocene evolution of the lower Mississippi River valley, southern Missouri to Arkansas. Geological Society of America Bulletin 112, 221–235.

Buylaert, J.P., Vandenberghe, D., Murray, A.S., HuotDe Corte, F., Van den Haute, P., 2007. Luminescence dating of old (>70 ka) Chinese loess: A comparison of single-aliquot OSL and IRSL techniques. Quaternary Geochronology 2, 9–14.

Bøtter-Jensen, L., Andersen, C.E., Duller, G.A.T., Murray, A.S., 2003. Developments in radiation, stimulation and observation facilities in luminescence measurements. Radiation Measurements 37, 535–541.

Catt, J.A., 1991. Soils as indicators of Quaternary climatic change in mid-latitude regions. Geoderma 51, 167–187.

Crowley, T.J., Kim, K.Y., 1994. Milankovitch Forcing of the Last Interglacial Sea Level. Science 265, 1566–1568.

Dorale, J.A., Lawrence Edwards, R., Ito, E., Gonzàlez, L.A., 1998. Climate and Vegetation History of the Midcontinent from 75 to 25 ka: A Speleothem Record from Crevice Cave, Missouri, USA. Science 282, 1871–1874.

Fairbanks, R.G., Mortlock, R.A., Chiu, T.C., Cao, L., Kaplan, A., Guilderson, T.P., Fairbanks, T.W., Bloom, A.L., Grootes, P.M., 2005. Radiocarbon calibration curve spanning 0 to 50,000 years BP based on paired Th-230/U-234/U-238 and C-14 dates on pristine corals. Quaternary Science Reviews 24, 1781–1796.

Follmer, L.R., 1983. Sangamon Geosol and Wisconsinan pedogenesis in the Midwestern United States. The Pleistocene. In: Porter, S.C. (Ed.), Late-Quaternary Environments of the United States, Vol. 1. University of Minnesota Press, Minneapolis, pp. 138–144.

Follmer, L.R., 1996. Loess studies in central United States: Evolution of concepts. Engineering Geology 45 (1-4), 287–304.

Forman, S.L., Pierson, J., 2002. Late Pleistocene luminescence chronology of loess deposition in the Missouri and Mississippi river valleys, United States. Paleogeography, Paleoclimatology. Paleoecology 186, 25–46.

Forman, S.L., Bettis Jr., E.A., Kemmis, T., Miller, B.B., 1992. Chronologic evidence for multiple periods of loess deposition during the late Pleistocene in the Missouri and Mississippi River Valleys, U.S.: Implications for the activity of the Laurentide Ice sheet. Paleogeography, Paleoclimatology, Paleoecology 93, 71–83.

Galbraith, R.F., Roberts, R.G., Laslett, G.M., Yoshida, H., Olley, J.M., 1999. Optical dating of single and multiple grains of quartz from Jinmium rock shelter, northern Australia: part I, experimental design and statistical models. Archaeometry 41, 339–364.

Grimley, D.A., Follmer, L.R., Hughes, R.E., Solheid, P.A., 2003. Modern, Sangamon and Yarmouth soil development in loess of unglaciated southwestern Illinois. Quaternary Science Reviews 22, 225–244.

Grimley, D.A., Larsen, D., Kaplan, S.W., Yansa, C.H., Brandon Curry, B., Oches, E.A., 2009. A multi-proxy palaeoecological and palaeoclimatic record within full glacial lacustrine deposits, western Tennessee, USA. Journal of Quaternary Science 24, 960–981.

Jacobs, Z., Roberts, R.G., Lachlan, T.J., Karkanas, P., Marean, C.W., Roberts, D.L., 2011. Development of the SAR TT-OSL procedure for dating Middle Pleistocene dune and shallow marine deposits along the southern Cape coast of South Afri~Quaternary Geochronology 6, 491–513.

Jain, M., Murray, A.S., Bøtter-Jensen, L., 2003. Characterisation of blue-light stimulated luminescence components in different quartz samples: implications for dose measurement. Radiation Measurements 37, 441–449.

Jain, M., Murray, A.S., Bøtter-Jensen, L., Wintle, A.G., 2005. A single-aliquot regenerative-dose method based on IR (1.49 eV) bleaching of the fast OSL component in quartz. Radiation Measurements 39, 309–318.

Kemp, R.A., 2001. Pedogenic modification of loess: significance for palaeoclimatic reconstructions. Earth-Science Reviews 54, 145–156.

Kim, J.C., Duller, G.A.T., Roberts, H.M., Wintle, A.G., Lee, Y.I., Yi, S.B., 2009. Dose dependence of thermally transferred optically stimulated luminescence signals in quartz. Radiation Measurements 44, 132–143.

Kim, J.C., Duller, G.A.T., Roberts, H.M., Wintle, A.G., Lee, Y.I., Yi, S.B., 2010. Re-evaluation of the chronology of the palaeolithic site at Jeongokri, Korea, using OSL and TT-OSL signals from quartz. Quaternary Geochronology 5, 365–370.

Lamothe, M., Auclair, M., Hamzaoui, C., Huot, S., 2003. Towards a prediction of long-term anomalous fading of feldspar IRSL. Radiation Measurements 37, 493–498.

Leigh, D.S., Knox, J.C., 1992. AMS Radiocarbon Age of the Upper Mississippi Valley Roxana Silt. Quaternary Research 39, 282–289.

Li, B., Li, S.H., Wintle, A.G., 2006. Observations of thermal transfer and the slow component of OSL signals from quartz. Radiation Measurements 41, 639–648.

Lisiecki, L.E., Raymo, M.E., 2005. A Pliocene-Pleistocene stack of 57 globally distributed benthic $\delta^{18}O$ records. Paleoceanography 20, PA1003.

Maat, P.B., Johnson, W.C., 1996. Thermoluminescence and new C-14 age estimates for late Quaternary loesses in southwestern Nebraska. Geomorphology 17, 115–128.

Markewich, H.W., Wysocki, D.A., Pavich, M.J., Rutledge, E.M., Millard, H.T., Rich, F.J., Maat, P.B., Rubin, M., McGeehin, J.P., 1998. Paleopedology plus TL, Be-10, and C-14 dating as tools in stratigraphic and paleoclimatic investigations, Mississippi River Valley, USA. Quaternary International 51-2, 143–167.

Marquardt, D.W., 1963. An algorithm for least-squares estimation of non-linear parameters. Journal of the Society for Industrial and Applied Mathematics 11, 431–441.

Mason, J.A., Swinehart, J.B., Hanson, P.R., Loope, D.B., Goble, R.J., Miao, X., Schmeisser, R.L., 2011. Late Pleistocene dune activity in the central Great Plains. USA. Quaternary Science Reviews 30, 3858–3870.

McKay, E.D., 1979. Wisconsinan loess stratigraphy of Illinois. In: Wisconsinan, Sangamonian and Illinoian stratigraphy in central Illinois. Illinois State Geological Survey Guidebook 13, 95–108.

Muhs, D.R., Bettis III, E.A., Aleinikoff, J.N., McGeehin, J.P., Beann, J., Skipp, G., Marshall, B.D., Roberts, H.M., Johnson, W.C., Benton, R., 2008. Origin and paleoclimatic significance of late Quaternary loess in Nebraska: Evidence from stratigraphy, chronology, sedimentology, and geochemistry. Geological Society of America Bulletin 120, 1378–1407.

Murray, A.S., Mejdahl, V., 1999. Regenerative dose single-aliquot and multiple aliquot (SARA) protocols using quartz from archaeological sites. Quaternary Science Reviews 18, 223–229.

Murray, A.S., Wintle, A.G., 2000. Luminescence dating of quartz using an improved single-aliquot regenerative-dose protocol. Radiation Measurements 32, 57–73.

Murray, A.S., Roberts, R.G., Wintle, A.G., 1997. Equivalent dose measurement using a single aliquot of quartz. Radiation Measurements 27, 171–184.

Murray, A.S., Buylaert, J.P., Thomsen, K.J., Jain, M., 2009. The effect of preheating on the IRSL signal from feldspar. Radiation Measurements 44, 554–559.

Oches, E.A., McCoy, W.D., Clark, P.U., 1996. Amino acid estimates of latitudinal temperature gradients and geochronology of loess deposition during the last glaciation, Mississippi Valley, United States. GSA Bulletin 108, 892–903.

Pagonis, V., Wintle, A.G., Chen, R., Wang, X.L., 2008. A theoretical model for a new dating protocol for quartz based on thermally transferred OSL (TT-OSL). Radiation Measurements 43, 704–708.

Pagonis, V., Adamiec, G., Athanassas, C., Chen, R., Baker, A., Larsen, M., Thompson, Z., 2011. Simulations of thermally transferred OSL signals in quartz: Accuracy and precision of the protocols for equivalent dose evaluation. Nuclear Instruments and Methods in Physics Research 269, 1431–1443.

Porat, N., Duller, G.A.T., Roberts, H.M., Wintle, A.G., 2009. A simplified SAR protocol for TT-OSL. Radiation Measurements 44, 538–542.

Prescott, J.R., Hutton, J.T., 1994. Cosmic ray contributions to dose rates for luminescence and ESR dating: large depths and long-term time variations. Radiation Measurements 23, 497–500.

Roberts, H.M., 2007. Assessing the effectiveness of the double-SAR protocol in isolating a luminescence signal dominated by quartz. Radiation Measurements 42, 1627–1636.

Roberts, H.M., Duller, G.A.T., 2004. Standardised growth curves for optical dating of sediment using multiple-grain aliquots. Radiation Measurements 38, 241–252.

Rodbell, D.T., Forman, S.L., Pierson, J., Lynn, W.C., 1997. Loess and paleosol stratigraphy, magnetic susceptibility and chronology of Mississippi Valley loess in western Tennessee. Geological Society of America Bulletin 109 (9), 1134–1148.

Rosenberg, T.M., Preusser, F., Wintle, A.G., 2011. A comparison of single and multiple aliquot TT-OSL data sets for sand-sized quartz from the Arabian Peninsula. Radiation Measurements 46, 573–579.

Singarayer, J.M., 2002. Linearly modulated optically stimulated luminescence of sedimentary quartz: physical mechanisms and implications for dating. Unpublished D. Phil. Thesis, University of Oxford.

Singarayer, J.M., Bailey, R.M., 2003. Further investigations of the quartz optically stimulated luminescence components using linear modulation. Radiation Measurements 37, 451–458.

Sjostrand, H., Prescott, J.R., 2002. Thick source alpha counting: the measurement of thorium. Ancient TL 20, 7–10.

Smith, B.W., Rhodes, E.J., 1994. Charge movements in quartz and their relevance to optical dating. Radiation Measurements 23, 329–333.

Snowden Jr., J.O., Priddy, R.R., 1968. Geology of Mississippi Valley Loess. Mississippi Geological, Economic and Topographic Survey Bulletin 111, 1–203.

Spooner, N.A., Questiaux, D.G., 2000. Kinetics of red, blue and UV thermoluminescence and optically-stimulated luminescence from quartz. Radiation Measurements 32, 659–666.

Steffen, D., Preusser, F., Schlunegger, F., 2009. OSL quartz age underestimation due to unstable signal components. Quaternary Geochronology 4, 353–362.

Stevens, T., Buylaert, J.-P., Murray, A.S., 2009. Towards development of a broadly-applicable SAR TT-OSL dating protocol for quartz. Radiation Measurements 44, 639–645.

Tsukamoto, S., Duller, G.A.T., Wintle, A.G., 2008. Characteristics of thermally transferred optically stimulated luminescence (TT-OSL) in quartz and its potential for dating sediments. Radiation Measurements 43, 1204–1218.

Wang, H., Lundstrom, C.C., Zhang, Z., Grimley, D.A., Balsam, W.L., 2009. A Mid-Late Quaternary loess-paleosol record in Simmons Farm in southern Illinois, USA. Quaternary Science Reviews 28, 93–106.

Wang, X.L., Lu, Y.C., Wintle, A.G., 2006. Recuperated OSL dating of fine-grained quartz in Chinese loess. Quaternary Geochronology 1, 89–100.

Wang, X.L., Wintle, A.G., Lu, Y.C., 2007. Testing a single-aliquot protocol for recuperated OSL dating. Radiation Measurements 42, 380–391.

Wang, X.L., Wintle, A.G., Adamiec, G., 2012. Improving the reliability of single-aliquot regenerative dose dating using a new method of data analysis. Quaternary Geochronology 9, 65–74.

Wintle, A.G., Huntley, D.J., 1982. Thermoluminescence dating of sediments. Quaternary Science Reviews 1, 31–53.

Wintle, A., Murray, A., 2006. A review of quartz optically stimulated luminescence characteristics and their relevance in single-aliquot regeneration dating protocols. Radiation Measurements 41, 369–391.